

# Design of a ZCT Inverter for a Brushless DC Motor - Simulation Results

B. Taleb  
School of Engineering & Logistics  
Charles Darwin University  
Darwin Australia 0909  
s994786@students.cdu.edu.au

K. Debnath  
School of Engineering & Logistics  
Charles Darwin University  
Darwin Australia 0909  
Kamal.Debnath@cdu.edu.au

D. Patterson  
University of Nebraska  
Lincoln Nebraska  
USA  
patterson@ieee.org

## ABSTRACT

*In this paper the implementation and the simulation of a new controller for the control of an axial flux brushless DC motor is analysed. The new controller has the features of operating on hard switching, soft switching with one switch or two switches Pulse width modulated (PWM). It uses a closed loop current control with the addition of three soft switching units. Each of the unit controls one phase of the ZCT inverter. After leaving the commutation logic unit whose role is to apply the current to the correct windings, in the correct direction, at the correct time, each signal goes through the soft switching unit, in order to soft switch the desired MOSFETs to be controlled. The current band is set to 5A, which gives a maximum switching frequency of 26 kHz. This occurs at half motor speed. In order to view the performance of the controller, it is simulated using the Matlab Simulink package. The currents in the three phases of the ZCT inverter, the gate pulses of the main switch  $S_1$  and auxiliary switches (lower  $S_{x1}$ , upper  $S_{x2}$ ) are all computed. During the commutation of the current from one phase to another, there is a small dip of current in the third phase. It can also be observed that  $S_{x1}$  is switched during the turn on of switch  $S_1$  and  $S_{x2}$  during its turn off. The computed resonant tank current  $i_x$  takes about two cycles to settle down. Its peak value is around 600 amps for a load current of 150 amps and this occurs at turn on, i.e. during the switching of the auxiliary switch  $S_{x1}$ . The maximum resonant current at the turn off transition is about 260A i.e. during the conduction of  $S_{x2}$ . The computed maximum voltage across the tank capacitor  $v_x$  is 120 V. This occurs at the turn off transition, and is about 30 % higher than the supply battery voltage. The computed waveform of the inverter in the X (Voltage) Y (current) Graph (State plane) during one whole cycle of the inverter shows a different cycle during the period of initial transition, and after that the cycle repeats to itself.*

## 1. INTRODUCTION

The application of brushless DC motors (BDCMs), of all types, is becoming of considerable importance particularly in EV systems. This is largely due to the benefits that these types of motor bring to the system, particularly in improvements in the reliability, ruggedness, volume, mass and efficiency [1-6]. The control of brushless dc motors depends on the ability to control the winding currents relative to the rotor's

position, to obtain the switching pattern according to a particular switching one. A BDCM is similar in construction to a permanent magnet (PM) synchronous machine. The sinewave PM brushless motor drive, also called the PM synchronous motor (PMSM) drive, is fed by sinewave current and uses continuous rotor position feedback signals to control the commutation. On the other hand, the square wave PM brushless motor drive, also called the PM brushless dc motor drive, is fed by a square wave current and uses discrete rotor position feedback signals to control the commutation. The ideal back emf and current waveforms of a BDCM are shown in Figure 1. Since the interaction between the square wave current and the trapezoidal magnetic flux in the motor can produce a larger average torque product than that produced by sine wave current and sine wave magnetic field, a higher average magnetisation of the magnetic material by a factor of around 1.3 will result. Thus a PM brushless dc motor drive possesses higher power density than the PM synchronous machine. The use of concentrated winding patterns in conjunction with trapezoidal flux distribution results in a trapezoidal induced back emf across each phase winding.

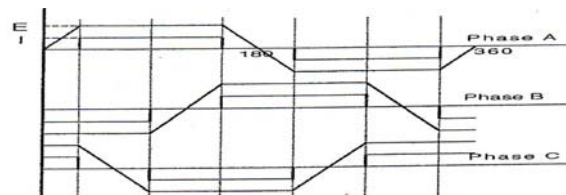


**Figure 1** Ideal trapezoidal back emf (E) and rectangular current (I) waveforms of a BDCM.

## 2. BRUSHLESS DC MOTOR CONTROL

The new controller is implemented as shown in Figure 2. It uses a closed loop current control, with the addition of three soft switching units. Each of the unit controls one phase of the ZCT inverter. After leaving the commutation logic unit whose role is to apply the current to the correct windings, in the correct direction, at the correct time, each signal goes through the soft switching unit, in order to soft switch the desired MOSFETs to be controlled. The current band is set to be 5A, which gives a maximum switching frequency of 26 kHz. This occurs at half motor speed. In order to view the performance of the ZCT inverter, it is simulated using the Matlab Simulink package software.

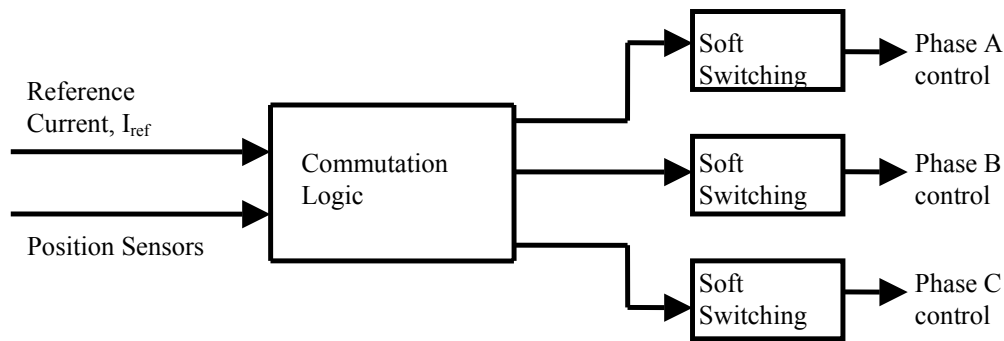


**Figure 2** Block diagram of the ZCT inverter

To simulate the brushless DC motor using the Simulink package the permanent magnet synchronous machine with sinusoidal flux distribution from the power system blockset library was used. The stator windings are connected in Wye to an internal neutral point. The first three inputs are the electrical connections to the machine's stator. The fourth input is the mechanical torque at the machine's shaft (Simulink signal). This input should normally be positive because the PMSM is usually used as a motor. The block outputs a vector containing the following ten variables (all currents flowing into the machine):

- 1-3: line currents  $i_a$ ,  $i_b$  and  $i_c$ .
- 4-5: q and d axis currents  $i_q$  and  $i_d$ .
- 6-7: q and d axis voltages  $v_q$  and  $v_d$ .
- 8: Rotor electrical speed  $\omega_e$ .
- 9: Rotor electrical angle  $\theta_e$
- 10: Electromagnetic torque  $T_e$ , into and out of the phases of the stator windings.

The values of the parameters of the machine resistance, and the inductances are taken respectively as ( $R = 0.028 \Omega$ ,  $L = 182 \mu\text{H}$ ). Three trapezoidal constant currents with a crest of 120 electrical degrees interval supply the machine. Hall effects sensors are used to capture the position of the rotor to eventually energize the correct phases. To realise the Hall effect signals an angle of rotation between 0 to 360 degrees is required. This was implemented by using the angle in rad/sec. The angle was divided by  $2\pi$ . The remainder function was used to obtain an angle between 0-360 degrees. The answer from the function was multiplied by 360 degrees before it was subtracted from 360 degrees. So, the output of this is an angle between 0-360 degrees. At any time only two phases of the motor winding carry current. Each phase conduct for 120 electrical degrees in every cycle and commutation takes place every  $60^\circ$ . This is known as six-step commutation or six-step control. Figure 3 shows the functional BDCM drive system with closed loop torque control. The motor is star connected and requires only six power switching devices. The position of the rotor which determines the flow of current is obtained from Hall effect sensors. Alternatively indirect position sensor can also be used but in the work reported in this paper only Hall effect sensors were used. Some of the major issues considered in designing the motor controller are:

- System efficiency maximization (the best tradeoffs between motor and inverter losses)
- Motor torque output maximization
- Flux level optimisation as a function of the requested performance
  - Smooth torque control over the entire range
  - Stability over the entire speed range

The BDCM drive system developed here for the control of the axial flux brushless DC motor uses a unipolar voltage-switching scheme. The frequency of the fully on switch is around 300Hz, which is the maximum frequency of the commutation. It was decided to soft switch only the upper switches, as efficiency is very important.

### 3. HYSTERISIS BAND CURRENT CONTROL

Pulse width modulation (PWM) is the method of choice in controlling power electronic circuits. In PWM, the voltage consists of a series of pulses of variable width. The average value of the voltage is controllable by varying the width of the pulse. The switching frequency (repetition frequency for the PWM signal) is chosen high enough so that the load cannot follow the individual switching events. Switching rather than linear operation of the power semi conductors is done in order to maximize the efficiency. In a typical case, the switching events react only on the average state of the switch. Modern electric drives and power supplies always operate in switched mode. Popular methods of switching modulation include Pulse Width Modulation (PWM) using a ramp comparison technique, Hysteresis band modulation, Delta modulation, etc [7-10]. The regulation of the motor currents can be achieved through the control of the duty cycle. For Hysteresis Band Modulation and Delta Modulation, the switching frequency is not constant. In the ramp comparison technique, the current error acts as the modulating wave and a triangle waveform acts as a carrier wave. The advantage of such a system is that it forces the inverter switching frequency to be the triangular waveform frequency. However this method has its shortcomings. Multiple crossings of the ramp can become a problem when the time rate of change of the current error exceeds that of the ramp. Hysteresis current control is the simplest and it is used in this work. The hysteresis comparator is used to impose a dead band or hysteresis around the reference current. This scheme provides excellent dynamic performance since it acts very quickly. An

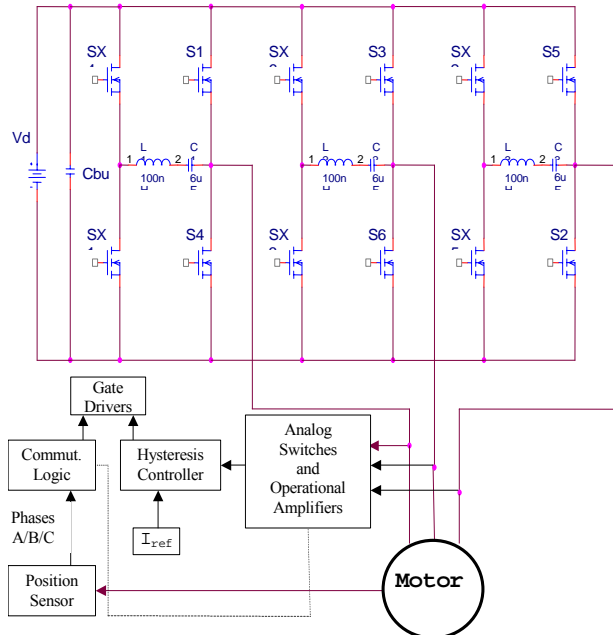


**Figure 3** A BDCM drive system with closed loop torque control

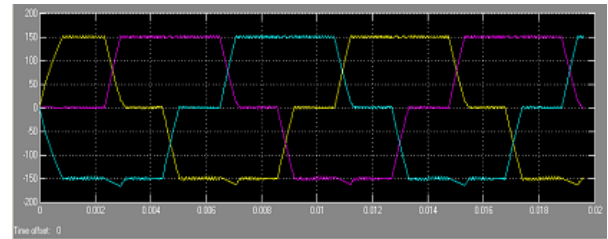
inherent peak current limiting capability is also provided. The operation of the current loop is absolutely stable, as the actual current always follows the current command. The main disadvantage of hysteresis current control with a fixed hysteresis band is that the switching frequency varies with both motor speeds and bus voltage. A hysteresis current PWM control, which consists of controlling the ON and OFF of the switches to keep the current within a band around the desired value, is used. A current  $I^*$  is the reference current waveform, i.e. the desired current,  $2\Delta I$  is the tolerance band,  $I^- = I^* - \Delta I$  is the lower band, and  $I^+ = I^* + \Delta I$  is the upper band. Whenever the current crosses the upper band, a switch is opened allowing the current to decay or discharge. Like wise whenever the current crosses the lower band, a switch is closed, forcing the current to climb in amplitude or charges the inductance. Clearly the rate at which the inductance involved charges or discharges influences the rate at which the switching occurs. In a motor drive, where the voltage across the inductance is a function of the difference between the supply voltage and back emf, the switching frequency will be low at low and high speeds. The switching frequency can be decreased by increasing the tolerance band. However this will increase the percentage ripple in the current. Some important aspects of this hysteresis PWM scheme are:

- Precise current control is possible as the tolerance bandwidth is a design parameter.
- The frequency at which switches change is not a design parameter. As a result the switching frequency can vary by an order of magnitude or more.
- Acoustic and electromagnetic noise is difficult to filter because their respective spectral components vary with the switching frequency.

This PWM method is more commonly implemented in motor drives where motor speed and load are constant.

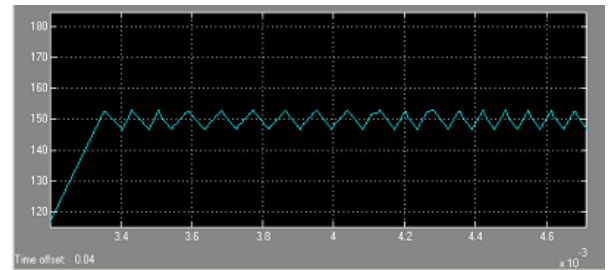
#### 4. SIMULATION RESULTS

The simulated currents in the three phases of the ZCT inverter are shown in Figure 4. During the commutation of the current from one phase to another, there is a small dip of current in the third phase.



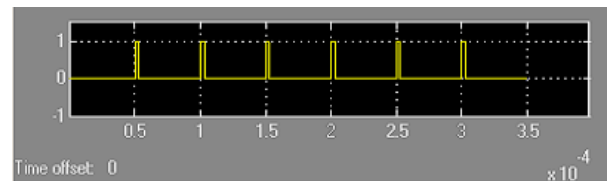
**Figure 4** Instantaneous phase currents of the ZCT inverter. Scale: Horiz: 0.002 sec/div, Vert: 50A/div

Figure 5 shows a current band of  $\pm 5$  A around the load current of 150 A.

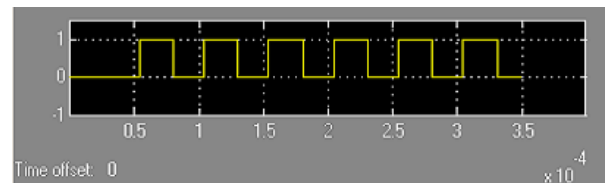


**Figure 5** Hysteresis band of current  
Scale: Horiz: 0.002 sec/div, Vert: 50A/div

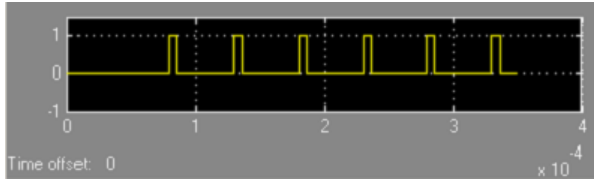
Figures 6, 7 and 8 show respectively the gate pulses for the auxiliary switches  $S_{x1}$  and  $S_{x2}$  and the main switch  $S_1$  for one phase. From these figures it can be observed that  $S_{x1}$  is switched on during the turn on of  $S_1$  and  $S_{x2}$  during its turn off.



**Figure 6** Pulses of the auxiliary switch  $S_{x1}$   
Scale: Horiz: 0.00005 sec/div

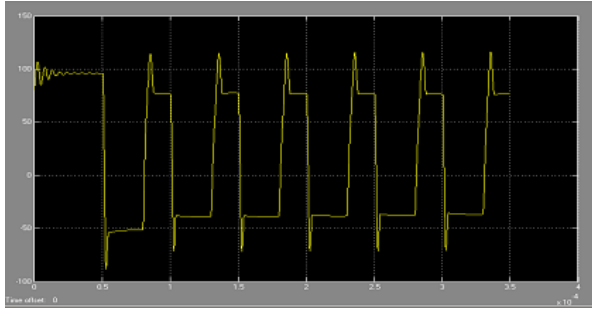


**Figure 7** Pulses of the main switch  $S_1$   
Scale: Horiz: 0.00005 sec/div



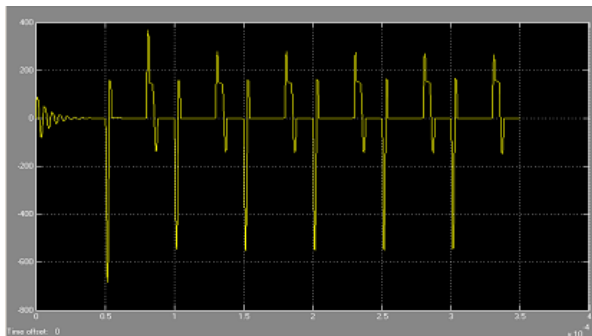
**Figure 8** Pulses of auxiliary switch  $S_{x2}$   
Scale: Horiz: 0.0001 sec/div

Figure 9 shows the voltage across the capacitor. For a supply battery voltage of 96V a maximum tank voltage  $v_x$  of 120V occurs during the turn off transition.



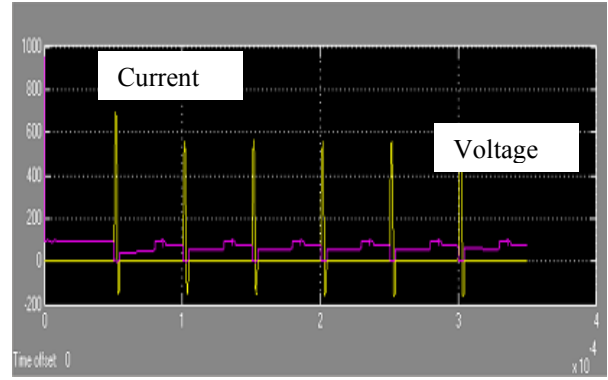
**Figure 9** Instantaneous voltage of the tank circuit  
Scale: Horiz: 0.00005 sec/div, Vert: 50V/div

Figure 10 shows the current in the resonant tank  $i_x$ . This current takes about two cycles to settle down. Its maximum value is around 600 amps for a load current of 150 amps and this occurs at the turn on transition i.e. during the switching of auxiliary switch  $S_{x1}$ . The maximum resonant current at the turn off transition is about 260 A i.e. during the switching of auxiliary switch  $S_{x2}$



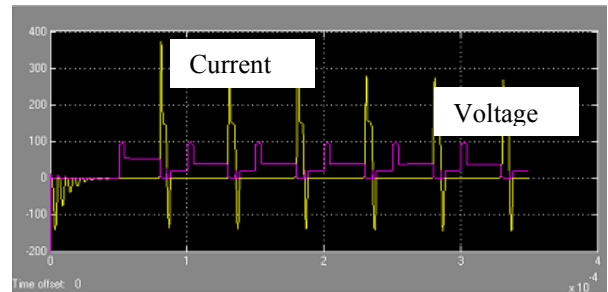
**Figure 10** Instantaneous current of the tank circuit.  
Scale: Horiz: 0.00005 sec/div, Vert: 200 A/div

Figure 11 shows the instantaneous voltage across and current waveforms of the auxiliary switch  $S_{x1}$ . The peak current is around 700 A. The device selection should be based on the peak current ability instead of the average current.



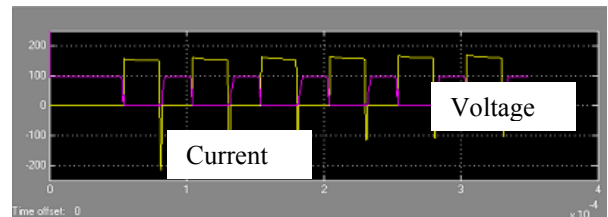
**Figure 11** Instantaneous voltage and current in of the auxiliary switch  $S_{x1}$ . Scale: Horiz: 0.00005 sec/div, Vert: 200V/div, 200A/div

Figure 12 shows the instantaneous voltage across and the current in the auxiliary switch  $S_{x2}$ . The peak current is about 400A and the switch should be chosen on its peak current capability.



**Figure 12** Instantaneous voltage and current of the auxiliary switch  $S_{x2}$ . Scale: Horiz: 0.00005 sec/div, Vert: 100V/div, 100A/div

Figure 13 shows the instantaneous voltage across and the current waveforms in the main switch  $S_1$ . The maximum current in the switch is just above 200A. Its selection should be based on the average current capability.



**Figure 13** Instantaneous voltage and current of the main switch  $S_1$ . Scale: Horiz: 0.0001sec/div, Vert: 100V/div, 100A/div

The ZCT inverter operation is analyzed by solving the LC 2<sup>nd</sup> order differential equations, step by step as shown in the paper Reference [11]. The state plane analysis which is a simple visualization tool to analyse resonant converters can be applied to study the ZCT inverter where the LC resonant circuit behaviour is a key part of its operation. By choosing the resonant inductor current  $i_x$  and the resonant capacitor voltage  $v_x$  as the state variables, from the sequence of topological stages we obtain the state plane trajectory shown in

Figure 14. As can be seen from this figure, during resonance, the state plane trajectory is part of a circle and the radius of the circle determines the resonant tank energy. In order to ensure the zero current turn off for the main switches, the resonant peak current at the turn off transition must be larger than the maximum load current period  $t_6$ - $t_7$ . The state plane analysis presented in Figure 14 shows the transition operating period (thin contour) and the normal operating condition (thick contour). The intervals  $t_1$ - $t_{10}$  give us an indication of the values of the voltage and the current during the different operation stages of the ZCT inverter.

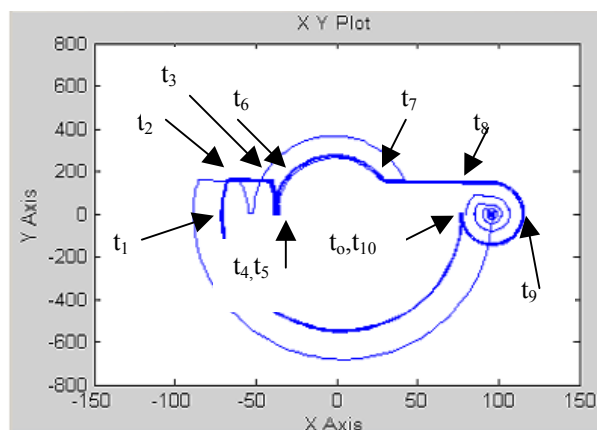


**Figure 14** X (Voltage) Y (Current) plot plane of the ZCT inverter

## 5. SUMMARY AND CONCLUSIONS

This paper shows that the ZCT PWM inverter can be applied for the control of an axial flux Brushless DC Motor. The axial flux BDCM is chosen because :

- It has a significant volume saving over the more usual radial flux geometry, for which much of the internal volume does not contribute to power output.
- A very simple technique for flux weakening that relies on mechanical adjustment of the air gap, and which does not impinge significantly on the efficiency becomes possible.

Among a substantial number of new topologies, the ZCT PWM inverter was chosen for the work reported in this paper due to its good characteristics. The voltage and current ratings of its main switches (Figure 13) and the body diodes are reduced. Each phase leg of the main circuit has a corresponding auxiliary circuit to assist the ZCT operation. Therefore, each switch is commutated independently so that any PWM scheme for hard switching counterparts can be directly employed without modification. A state plane analysis is also conducted for this ZCT inverter which is a simple visualization tool to analyze it. The thorough simulation of the controller of the ZCT inverter is conducted using MATLAB Simulink package. It gives a good insight on how the controller will perform especially the soft switching part of it. As can be seen from Figures 9 and 10, the maximum voltage across the tank capacitor occurs during the turn off transition,

whereas the maximum current in the tank inductor occurs during the turn on transition. The results from these simulations confirm the design parameters of the high power inductor as well as the specifications of the capacitors and the power MOSFETs. As stated earlier the selection of the auxiliary switches is based mainly on their peak current handling capability. Most of the beneficial functions of this ZCT PWM inverter were computed. These include the following promising features:

- Compared with the hard switching inverter, the turn on and turn off loss will be reduced.
- The voltage overshoot and the high frequency ringing at the turn off transition will be basically minimized.
- The resonant capacitor stress will be manageable
- The current and thermal stresses will be distributed evenly among the auxiliary devices.

## REFERENCES

- [1] Dean. Patterson and Rene. Spee, "The Design and Development of an Axial Flux Permanent Magnet Brushless DC Motor For Wheel Drive in a Solar Powered Vehicle," IEEE Transactions on Industry Applications, vol. 31, no. 5, September/October 1995, pp. 1054-1061.
- [2] D. J. Patterson, and J. B. Jermakian, "Contemporary Finite Element Analysis Techniques for Permanent Magnet Brushless DC Machines with Application to Axial Flux Traction Systems for Electric Vehicles," IEEE 1998, vol. 1 no.3, pp. 880-885.
- [3] D. J. Patterson, X Yan, and S. Camilleri, "A Very High Efficiency Controller For Axial Flux Permanent Magnet Wheel Drive in a Solar Powered Vehicle," Presented at the IEEE International conference on Power Electronics Drives and Energy Systems for Industrial Growth (PEDES'98), Perth, Australia, 1998.
- [4] S. Camilleri, D. J. Patterson, H. Pullen, "Development of a Silent Brushless DC Motor Drive," Presented at Australia Universities Power Engineering Conference (AUPEC), 1999, reprinted as a Journal paper in the Journal of Electrical and Electronics Engineering, Australia, Special Issue on Power Engineering, vol 20, no 1, 2000, pp 23-28
- [5] Paul. L. Chandler, and Dean J. Patterson, "Counting Losses in Very High Efficiency Machine Design," Journal of Renewable Energy 22 (2001), pp. 143-150
- [6] Francesco Profumo, Zheng Zhang, and Alberto Tenconi, "Axial Flux Machines Drives: A New Viable Solution for Electric Cars," IEEE Transactions on Industrial Electronics, vol. 44, no. 1, February 1997, pp-39-45.

- [7] M. Kheraluwala, D.M Divan, "Delta Modulation Strategies For Resonant Inverters," IEEE-PESC 1987, pp. 271-278.
- [8] M. Dawande, and G. k. Gopal, "Bang-Bang Current Control With predicted Switching Frequency for Switch –Mode Rectifiers," IEEE Transactions on Industrial Applications, vol. 46, no. 1, February 1999, pp. 61-66.
- [9] J.W. Dixon, and Ivan A. Leal, "Current Control Strategy for Brushless DC Motors Based on a Common DC Signal," IEEE Transactions on Power Electronics, vol. 17, no. 2, March 2002, pp. 232-240.
- [10] M. Azizur Rahman, John E. Quaicoe, and M. A. Choudhury, "Performance Analysis of Delta Modulated PWM Inverters," IEEE Transactions on Power Electronics, vol. PE-2, no. 3, July 1987, pp. 227-233.
- [11] B. Taleb, K. Debnath and D. Patterson, " Design of a ZCT Inverter for a Brushless DC Motor Theoretical Analysis," to be Presented in AUPEC, Tasmania, Australia, September 2005